PCCP

Accepted Manuscript

ROYAL SOCIETY OF CHEMISTRY

www.rsc.org/pccp

TOC

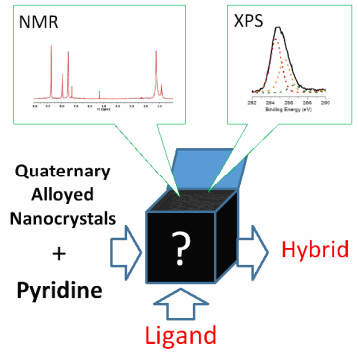

Detailed NMR and XPS studies of the exchange of initial ligands for pyridine in quaternary nanocrystals enabled us to demonstrate, for the first time, direct binding of this labile ligand to the nanocrystals' surface.

Journal Name

RSCPublishing

ARTICLE

Ligand exchange in quaternary alloyed nanocrystals – a spectroscopic study

Cite this: DOI: 10.1039/x0xx00000x

Received 00th January 2012,
Accepted 00th January 2012

DOI: 10.1039/x0xx00000x

www.rsc.org/

Grzegorz Gabka[a], Piotr Bujak[a*], Kamila Giedyk[a], Kamil Kotwica[a], Andrzej Ostrowski[a], Karolina Malinowska[b], Wojciech Lisowski[c], Janusz W. Sobczak[c] and Adam Pron[a]

Exchange of initial, predominantly stearate ligands for pyridine in the first step and butylamine (BA) or 11-mercaptoundecanoic acid (MUA) in the second one was studied for alloyed quaternary Cu-In-Zn-S nanocrystals. The NMR results enabled to demonstrate, for the first time, direct binding of pyridine labile ligand to the nanocrystals' surface as evidenced by paramagnetic shifts of the three signals attributed to its protons to 7.58, 7.95 and 8.75 ppm. XPS investigations indicated, in turn, a significant change in the composition of the nanocrystals surface upon the exchange of initial ligands for pyridine, which being enriched in indium in the 'as prepared" form became enriched in zinc after pyridine binding. This finding indicated that the first step of ligand exchange had to involve the removal of the surfacial layer enriched in indium with simultaneous exposure of a new, zinc-enriched layer. In the second ligand exchange step (replacement of pyridine with BA or MUA) the changes in the nanocrystals surface compositions were much less significant. The presence of zinc in the nanocrystals' surface layer turned out necessary for effective binding of pyridine as shown by a comparative study of ligand exchange in Cu-In-Zn-S, Ag-In-Zn-S and $CuInS_2$, carried out by complementary XPS and NMR investigations.

Introduction

Semiconducting nanocrystals can be considered as hybrid inorganic/organic materials consisting of an inorganic core surrounded by a shell of surfacial stabilizing ligands.[1,2] The inorganic core size and shape determine nanocrystals' physical properties (including quantum confinement effect) whereas the ligands play a crucial role in the interactions between the nanocrystals and their chemical environment and determine their technologically useful properties. Initial ligands, *i.e.* ligands intentionally added to the reaction mixture to stabilize as prepared nanocrystals, in addition of an anchoring functional group frequently contain long chains usually of alkyl-type, facilitating the dispersion of these nanoparticles in non-aqueous media. In order to modify surfacial properties of nanocrystals the initial ligands are frequently exchanged for functional ligands capable of interacting with a given analyte,[3] biomolecules[4,5] or other nanocrystals.[6]

One of the simplest and most widely used methods of ligand exchange is a two-step procedure in which the initial ligands are first exchanged for pyridine – a labile ligand, which in the next step is replaced with the target ligand.[7] Pyridine was used as an intermediate ligand for the modification of the surface of such nanocrystals as CdSe,[8] for example. Its further exchange for butyl- or octylamine enabled optimization of the parameters of nanocrystals-based solar cells.[9,10]

More recently, extensive research has begun on ternary and quaternary semiconducting nanocrystals which do not contain toxic metals. They are presently considered alternatives to cadmium and lead chalcogenides.[11,12] Among them alloyed Cu-In-Zn-S and Ag-In-Zn-S nanocrystals, fabricated from simple, commercially available precursors deserve special attention.[13-15] Modification of their preparation conditions enables precise control of their size and shape. As a consequence, their photo- and electroluminescent properties can be relatively easily tuned in a broad spectral range. The photoluminescence quantum yield (QY) is especially high in nonstoichiometric, alloyed Cu-In-Zn-S nanocrystals of high Zn and low Cu contents (Cu < In << Zn) in accordance with the donor-acceptor recombination mechanism[16,17] involving Cu(I) ions substituted by In(III) ones as well as sulfur vacancies as donor states and Cu(I) vacancies as acceptor states.[17]

The studies of initial ligands' exchange process for pyridine and in the next step for ligands such as short amines (butylamine, for example) is especially important in the view of nanocrystals application in photovoltaics and related fields.

Similarly, studies on introducing surfacial ligands which induce dispersion of nanocrystals in aqueous media. (11-mercaptoundecanoic acid (MUA) and dihydrolipoic acid (DHLA), L-cysteine and D-penicillamine, to name a few) are vital for all applications of non-toxic nanocrystals in biosensing.[18] For the identification of new ligands capped on the surface of nanocrystals NMR spectroscopy can be used,[19,20] frequently in combination with IR[20,21] and XPS.[22] However, spectroscopic studies on labile (pyridine) and the target ligand interactions with nanocrystals surface are surprisingly scarce[7] and spectroscopic interpretation of these phenomena is difficult. The work of Kolny-Olesiak et al.[10] can be considered here as an instructive example of a successful approach to this problem. These authors reported detailed spectroscopic characterization of pyridine-capped CdSe nanocrystals.

In this paper we report, for the first time, a direct spectroscopic evidence for binding of intermediate (pyridine) and final (butylamine or 11-mercaptoundecanoic acid) ligands on the surface of quaternary Cu-In-Zn-S and Ag-In-Zn-S nanocrystals. The investigation of these processes is important not only from the basic research point of view but also for practical reasons. It allows for an estimation of the ligand exchange degree in both processes (initial ligands – pyridine – final ligands). In addition, it is demonstrated that these processes are strongly dependent on the composition of the surficial layer.

2. Experimental Section

2.1 Materials

$CuCl_2 \times 2H_2O$, $AgNO_3$, sodium oleate (82%), indium(III) chloride (98%), indium(III) acetate (99.99%), zinc stearate (technical grade), 1-dodecanethiol (DDT, 98%), oleylamine (OLA, 70%), 1-octadecene (ODE, 90%), sulfur (99.5%), pyridine (anhydrous, 99.8%), n-butylamine (99.5%), 11-mercaptoundecanoic acid (MUA, 95%) were supplied by Sigma-Aldrich. The details of the synthesis of copper(II) oleate are described in the Supporting Information.

2.2 Preparation of Cu-In-Zn-S alloyed nanocrystals[14]

All operation were carried out under constant dry argon flow. In a typical synthesis of alloyed Cu-In-Zn-S nanocrystals, copper(II) oleate (0.032 g, 0.05 mmol), indium chloride (0.44 g, 1.9 mmol), zinc stearate (1.8 g, 2.8 mmol), and DDT (1.2 g, 5.9 mmol) were mixed with ODE in a three-neck flask. The mixture was heated to 210 °C until a homogenous solution was formed. Then sulfur (15 mg, 0.47 mmol) dissolved in 1 mL of OLA was quickly injected into the reaction solution. After being kept at temperature 210 °C for 15 minutes, the solution was heated at 230 °C for another 5 minutes and then cooled to room temperature. The crude reaction mixture was mixed with 1 equiv. volume of chloroform and 4 equiv. of acetone and finally centrifuged (7000 rpm) for 10 minutes. The supernatant was discarded. The precipitate was washed three times in the same manner and then the nanocrystals redispersed in chloroform.

2.3 Preparation of Ag-In-Zn-S alloyed nanocrystals[15]

Silver nitrate (0.020 g, 0.11 mmol), indium(III) chloride (0.59 mmol, 0.132 g), zinc stearate (1.2 g, 1.9 mmol) and DDT (0.600 g, 2.9 mmol) were mixed with ODE in a three-neck flask. The mixture was heated under argon flow to 150 °C until a homogenous solution was formed. Then sulfur (15 mg, 0.47 mmol) dissolved in 1 mL of OLA was quickly injected into the reaction solution. The temperature was raised to 180 °C, and the mixture was kept at this temperature for 60 minutes. After the mixture was cooled to room temperature, toluene (20 mL) was added, and the reaction mixture was centrifuged – the isolated black precipitate was separated. The supernatant was treated with 30 mL of acetone leading to the precipitation of the desired fraction of nanocrystals. The nanocrystals were separated by centrifugation (7000 rpm, 10 min) and then redispersed in chloroform.

2.4 Preparation of Cu-In-S nanocrystals

Copper(II) oleate (0.5 mmol, 0.314 g) and 1-dodecanethiol (1 mmol, 0.202 g) dissolved in 15 mL of ODE were placed in a reaction vessel and subsequently heated to 230 °C. In parallel, 0.5 mmol (0.146 g) of indium(III) acetate dissolved in 8 mL of ODE, were placed in a second reaction vessel, then heated to 120 °C. This mixture was then transferred to the first reaction vessel, containing copper and sulfur precursors, continuously kept at the temperature of 230 °C. The temperature was then raised to 255 °C and the reaction mixture was heated at this temperature for additional 90 minutes. The reaction mixture was cooled to room temperature, and nanocrystals were precipitated by adding acetone and then collected by centrifugation (7000 rpm, 10 min). The final product was dispersed in chloroform for further characterization.

2.5 Ligand exchange for pyridine

Quaternary or ternary nanocrystals, prepared as described above, were dissolved in 10 mL of chloroform then mixed with 15 mL of acetic acid and stirred for 15 minutes. In the next step 30 mL of methanol was added and the resulting slurry was centrifuged. The precipitated nanocrystals were washed with 20 ml of methanol to remove excess of the acid and centrifuged again. As prepared nanocrystals were transferred to a three-neck flask and 15 mL of pyridine was added. The mixture was then heated at 110°C under argon atmosphere for 2h. After cooling the solution was mixed with 40 mL of hexane leading to the precipitation of nanocrystals, which were separated by centrifugation. Solid residue was washed with 15 mL of methanol to remove excess pyridine and then redispersed in 10 mL of chloroform.

2.6 Ligand exchange for n-butylamine

Chloroform solution of nanocrystals capped with pyridine was evaporated, solid residue was dissolved in 10 ml of n-butylamine. As obtained solution was stirred at room temperature overnight. Nanocrystals were precipitated with acetone, centrifuged and redispersed in chloroform.

2.7 Ligand exchange for 11-mercaptoundecanoic acid

0.5 g (2.29 mmol) of 11-mercaptoundecanoic acid and 0.1 g (2.5 mmol) of NaOH were dissolved in 10 mL of water and transferred to a three-neck flask. Separately, chloroform

solution of nanocrystals capped with pyridine was evaporated, solid residue was dissolved in 5 mL of toluene and then injected into the first solution. As obtained two-phase mixture was heated at 100°C for 3h under argon atmosphere. At this point the organic layer became colorless. After cooling the reaction mixture was centrifuged to obtain complete phase separation – any solids and the organic phase were discarded. Water solution was then mixed with 20 mL of acetone which lead to the precipitation of nanocrystals. After the centrifugation nanocrystals were redispersed in 10 ml of water.

2.8 Characterization

^{1}H NMR spectra were recorded on a Varian Mercury (400 MHz) spectrometer and referenced with respect to tetramethylsilane and solvents. Solid state FT-IR spectra were recorded on a Nicolet 6700 FTIR-ATR spectrometer (Thermo Scientific). The material for XPS analysis was preliminary dispersed in chloroform (or water), then deposited on a Si(100) substrate and dried at room temperature. X-ray photoelectron spectroscopy (XPS) experiments were performed in a PHI 5000 VersaProbe - Scanning ESCA Microprobe (ULVAC-PHI, Japan/USA) instrument at the base pressure below 5×10^{-9} mbar. The XPS spectra were recorded using monochromatic Al-Kα radiation (hν = 1486.6 eV) from an X-ray source operating at 100 µm spot size, 25 W and 15 kV. Both survey and high-resolution (HR) XPS spectra were collected with the analyzer pass energy of 117.4 eV and 23.5 eV and the energy step size of 0.4 and 0.1 eV, respectively. Casa XPS software (v. 2.3.16) was used to evaluate the XPS data. Shirley background subtraction and peak fitting with Gaussian–Lorentzian-shaped profiles was performed. Binding energy scale was referenced to the C 1s peak with BE = 284.6 eV. For quantification the PHI Multipak sensitivity factors and determined transmission function of the spectrometer were used. X-ray diffraction patterns were recorded on a Seifert HZG-4 automated diffractometer using Cu $K\alpha_{1,2}$ radiation (1.5418 Å). The data were collected in the Brag-Brentano (θ/2θ) horizontal geometry (flat reflection mode) between 10 and 70° (2θ) in 0.04° steps, at 10 s·step^{-1}. The optics of the HZG–4 diffractometer was a system of primary Soller slits between the X–ray tube and the fixed aperture slit of 2.0 mm. One scattered–radiation slit of 2 mm was placed after the sample, followed by the detector slit of 0.2 mm. The X-ray tube operated at 40 kV and 40 mA. TEM analysis were performed on Zeiss Libra 120 electron microscope operating at 120 kV. Elemental compositions of the prepared nanocrystals were determined by energy-dispersive spectroscopy. Absorption spectra were run on a Shimadzu UV-2700 spectrophotometer. Steady-state fluorescence was recorded using Edinburgh FS 900 CDT fluorometer (Edinburgh Analytical Instruments).

Results and Discussion

For the purpose of spectroscopic studies of surfacial ligands-nanocrystal interactions, described in this paper, alloyed Cu-In-Zn-S nanocrystals were prepared following the procedure elaborated by Zhang et al.[16] (for details see Experimental section). It relies on the injection of sulfur solution in oleylamine (OLA) to a mixture of standard commercial precursors in 1-octadecene (ODE). By changing the molar ratio of precursors (copper(II) oleate, indium(III) chloride, zinc stearate and 1-dodecanethiol (DDT)) it is possible to obtain zinc blende-type spherical nanocrystals of 2 to 3 nm in size. The detailed characterization of the nanocrystals by XRD, TEM, EDS, UV-vis spectroscopy and fluorometry can be found in the ESI†. NMR, IR and XPS studies were carried out for alloyed nanocrystals of the following composition Cu:In:Zn = 1:15:24 (as determined by EDS) which were obtained from the above mentioned precursors taken in a molar ratio Cu:In:Zn = 1:38:56. These nanocrystals feature an emission peak of λ_{max} of 513 nm and a Stokes shift of 150 nm, in accordance with previous findings.[11]

The exchange of initial ligands for pyridine was carried out in two steps. First, the colloidal dispersion of nanocrystals in chloroform was treated with acetic acid with the goal to remove the excess of stearate anions. In the second step the precipitated nanocrystals were mixed with pyridine. The resulting mixture was refluxed for 2 h. After the precipitation with hexane and removal of the excess of pyridine the nanocrystals were redispersed in chloroform. It should be stressed that the use of acetic acid was essential. Although the same effect could be obtained without the addition of acetic acid, the reproducibility was, however, poor. Attempts of application of stronger acids resulted in nanocrystals' degradation.

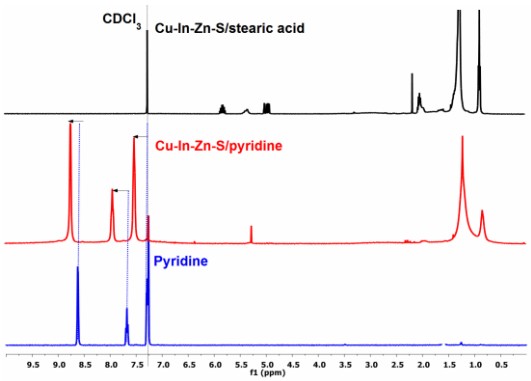

Fig. 1 ^{1}H NMR spectra of alloyed Cu-In-Zn-S nanocrystals (Cu:In:Zn = 1:15:24) before and after the exchange of initial capping ligands for pyridine. Pyridine spectrum is shown for comparison.

In Figure 1 ^{1}H NMR spectrum of nanocrystals capped with initial ligands is shown together with the corresponding spectrum registered after the exchange of these ligands for pyridine. The spectrum of pure pyridine is added for better comparison. In the spectrum of Cu-In-Zn-S nanocrystals capped with initial ligands lines characteristic of stearic acid and ODE coexist with those corresponding to minute amounts of OLA. All these ligands originate from the reaction mixture used for the preparation of nanocrystals. In particular, in the spectral range 4.90 - 5.90 ppm signals ascribed to olefinic protons in ODE (-CH=CH_2) and OLA (-CH=CH-) can be found. In the aliphatic part of the spectrum three groups of

signals can be distinguished: i) a multiplet at 0.86 - 0.89 ppm which has its origin in the overlap of three triplets originating from three nonequivalent methyl groups; ii) an additional intensive multiplet in the spectral range 1.20 - 1.35 ppm ascribed to methylene protons in aliphatic chains; iii) a third multiplet attributed to protons of α-CH_2 groups next to the double bond in ODE and OLA as well as adjacent to the carboxylic group of stearic acid.

After the exchange of the initial ligands for pyridine, the signals originating from ODE and OLA disappear whereas those attributed to stearic acid are still visible, indicating an incomplete ligand exchange. The ratio pyridine/stearic acid is 2:1, as deduced from the integration of the corresponding lines. Three signals, unequivocally attributed to pyridine protons are located at 7.58, 7.95 and 8.75 ppm *i.e.* they undergo a paramagnetic shift upon binding to the nanocrystal's surface since in the spectrum of pure pyridine the corresponding NMR lines can be found at 7.29, 7.68 and 8.62 ppm. This shift can therefore be considered as a manifestation of electron density lowering in the molecule, induced by its binding to the nanocrystal's surface. No peaks originating from noncoordinated pyridine can be found.

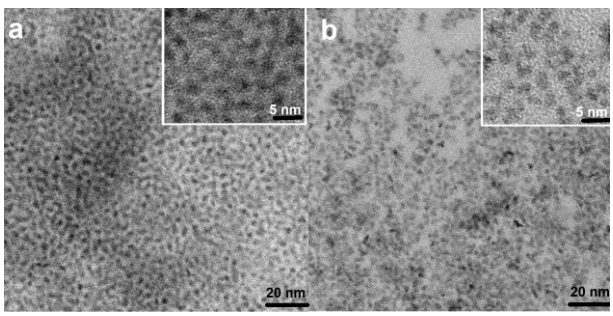

Fig. 2 TEM and enlarged TEM images of the same batch of alloyed Cu-In-Zn-S nanocrystals (Cu:In:Zn = 1:15:24) before (a) and after (b) the exchange of initial capping ligands for pyridine.

Surface binding of pyridine is additionally corroborated by IR spectroscopy (see Fig.S6 in the ESI†) through the appearance of diagnostic bands at 1617 and 1451 cm^{-1} (skeletal deformations region) as well as at 752 and 707 cm^{-1} (CH out of plane deformations region). The size and the shape of nanocrystals (spherical of 2-3 nm size) are not affected by the ligand exchange process, as evidenced by Figure 2 which compares images of initial ligand- and pyridine-capped alloyed Cu-In-Zn-S nanocrystals.

The second step of the ligand exchange process, *i.e.* replacement of labile pyridine ligands with n-butylamine (BA) or 11-mercaptoundecanoic acid (MUA) was also studied by ^1H NMR. In Figures 3 and 4 ^1H NMR spectra of dispersions of alloyed Cu-In-Zn-S nanocrystals, registered after the exchange of pyridine for BA and MUA, respectively, are presented. It can be noted that in both cases signals originating from the presence of pyridine totally disappeared, confirming high lability of this ligand both in nonpolar and polar media.

The signal corresponding to the methylene group adjacent to the amine one ($-CH_2NH_2$) is significantly broadened and paramagnetically shifted (~2.83 ppm) with respect to the corresponding signal in pure amine (2.67 ppm). Again, this can be taken as a spectroscopic manifestation of a decrease in the molecule electron density, induced by BA binding to the surface of a nanocrystal. An opposite effect is observed in the case of MUA-capped nanocrystals. In this ligand two anchoring groups can be distinguished, namely -SH and -COOH. The signal originating from methylene protons of the CH_2SH moiety (2.34 ppm) is diamagnetically shifted as compared to the case of pure MUA (2.49 ppm), indicating an increase of the electron density in coordinated MUA and pointing out that thiols are coordinated in their anionic (thiolate) form.[18] This is further corroborated by the presence of a broad band in the 3000 -3700 cm^{-1} region of the IR spectrum of MUA-capped nanocrystals (see Fig.S9 in the ESI†). This band is characteristic of undissociated carboxylic group,[23] hence confirming the coordination of MUA *via* the thiolate moiety.

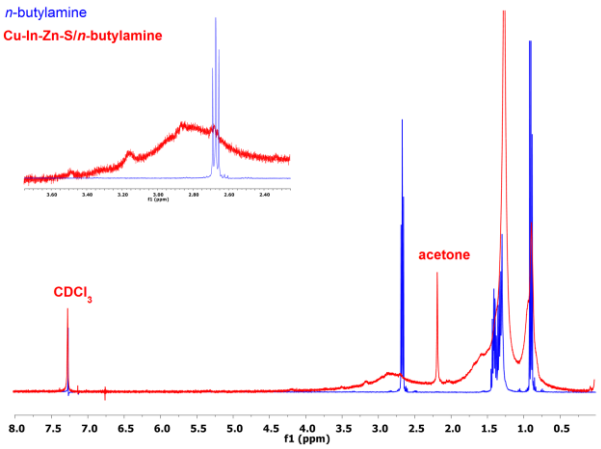

Fig. 3 ^1H NMR spectrum of $CDCl_3$ dispersion of Cu-In-Zn-S nanocrystals (Cu:In:Zn = 1:15:24) capped with n-butylamine (BA). The spectrum of pure BA is shown for comparison.

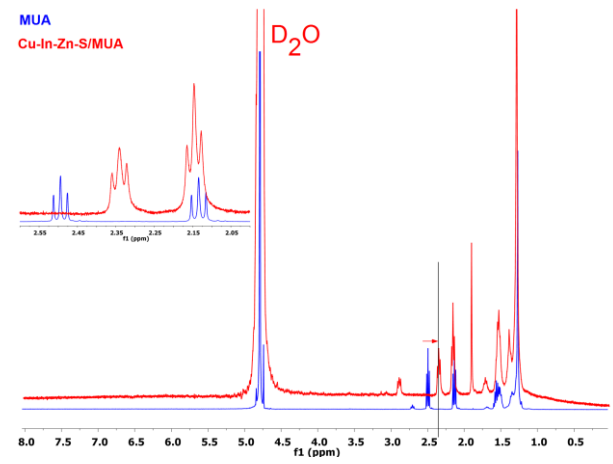

Fig. 4 1H NMR spectrum of D2O dispersion of Cu-In-Zn-S nanocrystals (Cu:In:Zn = 1:15:24) capped with 11-mercaptoundecanoic acid (MUA). The spectrum of pure MUA (pH = 9.0) is shown for comparison.

XPS is a very suitable spectroscopic technique for studying changes in the surfacial composition caused by ligands exchange. A complete set of survey spectra of Cu-In-Zn-S nanocrystals capped with initial ligands, pyridine, BA and MUA, together with high resolution spectra of the elements constituting the nanocrystal's surface and the capping ligands, are presented in the ESI† (Fig.S10-S17). Changes in surfacial composition, induced by the ligands exchange process are presented in Table 1.

These changes can be clearly correlated with the chemical constitution of the ligand. For nanocrystals capped with initial ligands which are a mixture of compounds containing long alkyl substituents the molar content of C is the highest, approaching 93 mol.%. Upon their exchange for pyridine mol.% of C significantly drops, consistent with a smaller number of carbon atoms in the individual ligand. Further drop in the carbon content is observed for nanocrystals capped with BA *i.e.* the ligand which introduces only four carbon atoms per molecule. Molar content of C again increases for MUA-capped nanocrystals consistent with a larger number on C atoms in an individual MUA molecule.

Table 1 Compositions of the surface and ligand layer in alloyed Cu-In-Zn-S nanocrystals capped with different ligands as determined by XPS spectroscopy

	mol.%C	mol.%O	mol.%N	mol.%S	Cu/In/Zn*
CuInZnS	92.8	3.6	0	1.4	-/1.7/1.0
CuInZnS/pyridine	60.6	7.4	1.1	16.8	1.0/4.8/31.1
CuInZnS/BA	48.6	9.7	3.2	20.3	1.0/5.0/28.2
CuInZnS/MUA	72.0	17.6	0	8.1	1.0/8.0/26.8

* Cu/In/Zn molar ratio

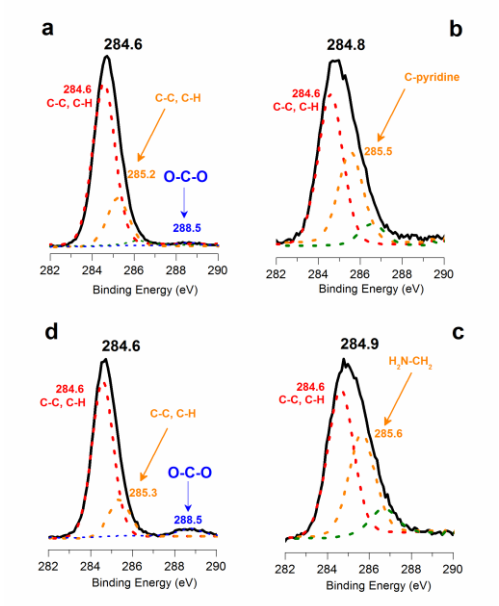

Fig. 5 High-resolution C1s XPS spectra of (a) stearic acid-, (b) pyridine-, (c) n-butylamine-, (d) MUA-capped Cu-In-Zn-S nanocrystals.

Exchange of ligands induces significant changes in the high resolution C1s spectra of the studied nanocrystals (see Figure 5). The spectrum of initial ligands-capped nanocrystals (Fig. 5a) is characterized by a dominant peak at 284.6 eV, which originate from aliphatic groups in 1-octadecene and stearic acid.[24] A weaker peak at 285.3 eV is characteristic of carbon atoms located close to the carboxylic group whereas a very weak line at 288.5 eV corresponds to the carboxylic carbon atom.[24] Upon exchange of initial ligands for pyridine (Fig. 5b) a strong component at 285.5 eV appears - characteristic of the pyridine ring.[25] The presence of pyridine is also manifested by the appearance of nitrogen in the surface analysis (see Table 1 and Figure S13 in the ESI†). However, the consequence of these surface modifications is partial quenching of the photoluminescence combined with a change in the emission spectrum maximum. (Figure S18 in the ESI†)

Exchange of pyridine for BA does not change the C1s spectrum to a large extent yielding a clear line of carbons in an amine-type moiety, exchange for MUA yields, in turn, a C1s spectrum which is similar to that recorded for nanocrystals stabilized with the initial ligands (compared Fig. 5a and d). This is not unexpected since both ligands are carboxylic acids with long aliphatic substituents, although MUA additionally contains a thiol group. Its presence is manifested in the S2p spectra.

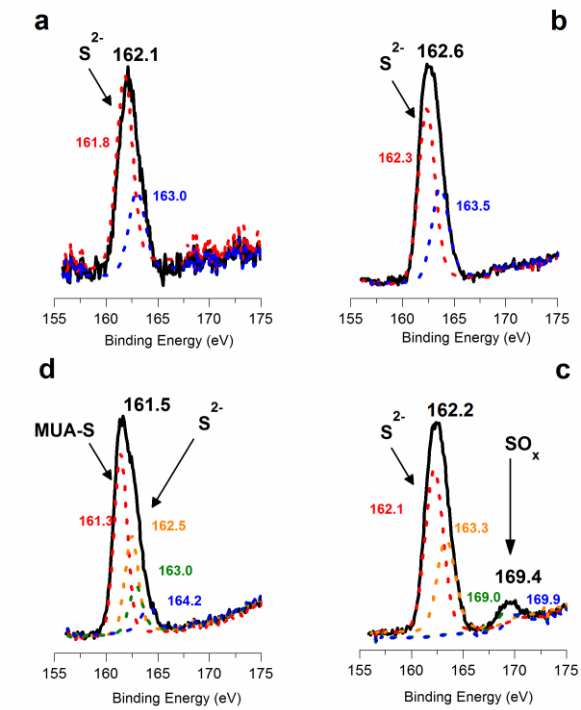

Fig. 6 High-resolution S2p XPS spectra of (a) stearic acid-, (b) pyridine-, (c) n-butylamine-, (d) MUA-capped Cu-In-Zn-S nanocrystals.

The spectra S2p of nanocrystals capped with initial ligands and after their exchange for pyridine are very similar and characteristic of S^{2-} ions of the inorganic core (see Figure 6a and 6b).[26] In the spectrum of BA-capped nanocrystals, in addition to peaks characteristic of S^{2-}, a new peak of weak

intensity appears at 169.4 eV (Fig. 6c). Since this peak is characteristic of SO_x^{2-} (x = 3,4), it can be postulated that the exchange of pyridine for BA is accompanied by the oxidation of a small part of sulfide to sulfite or sulfate. Similar results have been reported for PbS nanocrystals in which the presence of aliphatic amines induced the formation of $PbSO_3$ and $PbSO_4$ surfacial layers, improving parameters of the resulting photodetectors.[27]

For MUA-capped nanocrystals a clear shift of the dominant S2p peak towards lower binding energies, as compared to the case of nanocrystals capped with initial ligands, seems to indicate that MUA is bound to the nanocrystal surface via the thiol group. (Figure 6d) This is consistent with previous findings concerning the orientation of MUA with respect to the nanocrystals surface.[28] MUA attached to the surface of nanocrystals is however hydrated as evidenced by a distinct peak 535.5 eV in the O1s spectrum, which can be attributed to water molecules.[29]

XPS investigations of the ligands are fully consistent with the NMR data and reflect their chemical nature. However, it is equally important to determine the chemical composition of the inorganic core surface and the effect of the ligand exchange on this composition. A comparison of the ratio of metals derived from EDS (Cu:In:Zn=1:15:24) and XPS (Cu:In:Zn=0:1.7:1.0) in nanocrystals capped with initial ligands proves, that the nanocrystals volume composition differs from their surface composition. The surface is enriched in indium and contains very small amounts of copper (below the detection limit). In the bulk, in turn, zinc is the dominant element. This result unequivocally corroborates previous findings concerning effective diffusion of zinc into the bulk of nanocrystals with simultaneous replacement of indium and copper in the crystal lattice. As a consequence of this process the size of nanocrystals diminishes.[30,31] After the initial ligands exchange for pyridine the composition of the surfacial layer of the inorganic core drastically changes and becomes strongly enriched in zinc, simultaneously copper becomes detectable (Cu:In:Zn = 1.0:4.8:31.1 by XPS). In particular two lines at 952.5 eV and 932.7 eV appear in the Cu2p spectrum (see Fig.S16 in the ESI†), corresponding to Cu(II).[32] It can be therefore supposed that the introduction of pyridine ligands may involve removal of the surfacial layer enriched in indium with simultaneous exposure of a new, zinc-enriched layer which easily binds pyridine molecules. Note that the consecutive ligand exchange to yield BA- or MUA-capped Cu-In-Zn-S nanocrystals does not induce further profound surface composition changes (see data collected in Table 1).

For all nanocrystals studied, independently of the capping ligands nature, the binding energies, derived from the In3d and Zn2p spectra, are typical of alloyed Cu-In-Zn-S nanocrystals (see Fig. S14 and S17 in the ESI†).[30,31] The observed small differences in the binding energy values (never exceeding 1.0 eV) originate from differences in the composition of the inorganic core surfacial layer. No lines indicating the formation of new phases such as ZnO or In_2O_3 could be detected.[24]

This set of XPS data seems to indicate that the presence of zinc is necessary for an effective replacement of initial ligands with labile pyridine ligands in the studied nanocrystals. To verify whether this phenomenon is more general we have studied by ^{1}H NMR the exchange of initial ligands for pyridine in $CuInS_2$ and alloyed Ag-In-Zn-S nanocrystals. The obtained spectra are shown in Fig. S22 and S26 of ESI†. For zinc-free $CuInS_2$ no pyridine binding could be spectroscopically detected whereas for zinc-containing Ag-In-Zn-S three diagnostic pyridine lines underwent the same chemical shift as in the case of Cu-In-Zn-S nanocrystals.

Conclusions

To summarize, we have studied the process of initial ligand exchange for pyridine in alloyed quaternary nanocrystals Cu-In-Zn-S and Ag-In-Zn-S, proving, for the first time, direct pyridine binding to the nanocrystal surface as evidenced by a paramagnetic shift of all three pyridine lines in the NMR spectra of pyridine-capped nanocrystals. We have also demonstrated that the presence of zinc at the nanocrystal's surface is necessary for binding labile pyridine ligands. In these conditions further exchange of labile pyridine for butyl amine (BA) (or ligands inducing dispersion of nanocrystals in aqueous media such as mercaptoundecanoic acid, MUA) is complete as evidenced by NMR spectroscopy and corroborated by XPS studies.

Acknowledgements

This research was carried out in the framework of the project entitled "New solution processable organic and hybrid (organic/inorganic) functional materials for electronics, optoelectronics and spintronics" (Contract No. TEAM/2011-8/6), which is operated within the Foundation for the Polish Science Team Programme cofinanced by the EU European Regional Development Fund. The TEM images were obtained using the equipment purchased within CePT Project No. POIG.02.02.00-14-024/08-00.

Notes and References

[a]Faculty of Chemistry, Warsaw University of Technology, Noakowskiego 3, 00-664 Warsaw, Poland. E-mail: piotrbujakchem@poczta.onet.pl.
[b]Faculty of Chemistry, University of Warsaw, Pasteura 1, 02-093-Warsaw, Poland.
[c]Institute of Physical Chemistry, Polish Academy of Science, Kasprzaka 44/52, 01-224 Warsaw, Poland.

† Electronic Supplementary Information (ESI) available: [Detailed of characterization of quaternary (Cu-In-Zn-S and Ag-In-Zn-S) and ternary (Cu-In-S) nanocrystals. ^{1}H NMR, IR and XPS spectra of nanocrystals before and after the ligand exchange]. See DOI: 10.1039/b000000x/

1 C. B. Murray, D. J. Norris, M. G. Bawendi, *J. Am. Chem. Soc.*, 1993, **115**, 8706-8715.
2 C. de Mello Donegá, P. Liljeroth, D. Vanmaekelbergh, *Small*, 2005, **1**, 1152-1162.
3 J. M. Haremza, M. A. Hahn, T. D. Krauss, S. Chen, J. Calcines, *Nano Lett.*, 2002, **2**, 1253-1258.

4 X. Li, Y. Zhou, Z. Zheng, X. Yue, Z. Dai, S. Liu, Z. Tang, *Langmuir*, 2009, **25**, 6580-6586.
5 G. Palui, F. Aldeek, W. Wang and H. Mattoussi, *Chem. Soc. Rev.*, 2014, DOI: 10.1039/c4cs00124a
6 G. Tikhomirov, S. Hoogland, P. E. Lee, A. Fischer, E. H. Sargent, S. O. Kelley, *Nat. Nanotechnol.*, 2011, **6**, 485-490.
7 M. Green, *J. Mater. Chem.*, 2010, **20**, 5797-5809.
8 W. U. Huynh, J. J. Dittmer, A. P. Alivisatos, *Science*, 2002, **295**, 2425-2427.
9 N. Radychev, I. Lokteva, F. Witt, J. Kolny-Olesiak, H. Borchert, J. Parisi, *J. Phys. Chem. C*, 2011, **115**, 14111-14122.
10 I. Lokteva, N. Radychev, F. Witt, H. Borchert, J. Parisi and J. Kolny-Olesiak, *J. Phys. Chem. C*, 2010, **114**, 12784-12791.
11 H. Zhong, Z. Bai, B. Zou, *J. Phys. Chem. Lett.*, 2012, **3**, 3167-3175.
12 D. Aldakov, A. Lefrançois, P. Reiss, *J. Mater. Chem C*, 2013, **1**, 3756-3776.
13 D. Pan, D. Weng, X. Wang, Q. Xiao, W. Chen, C. Xu, Z. Yang, Y. Lu, *Chem. Commun.*, 2009, 4221-4223.
14 J. Zhang, R. Xie, W. Yang, *Chem. Mater.*, 2011, **23**, 3357-3361.
15 G. Gabka, P. Bujak, K. Giedyk, A. Ostrowski, K. Malinowska, J. Herbich, B. Golec, I. Wielgus, A. Pron, *Inorg. Chem.*, 2014, **53**, 5002-5012.
16 H. Zhong, Y. Zhou, M. Ye, Y. He, J. Ye, C. He, C. Yang, Y. Li, *Chem. Mater.*, 2008, **20**, 6434-6443.
17 D. E. Nam, W. S. Song, H. Yang, *J. Colloid Interf. Sci.*, 2011, **361**, 491-496.
18 S. Tamang, G. Beaune, I. Texier, P. Reiss, *ACS Nano*, 2011, **5**, 9392-9402.
19 Z. Hens, J. C. Martins, *Chem. Mater.*, 2013, **25**, 1211-1221.
20 E. Tavasoli, Y. Guo, P. Kunal, J. Grajeda, A. Gerber and J. Vela, *Chem. Mater.*, 2012, **24**, 4231-4241.
21 B. von Holt, S. Kudera, A. Weiss, T. E. Schrader, L. Manna, W. J. Parak, M. Braun, *J. Mater. Chem.*, 2008, **18**, 2728-2732.
22 A. Lobo, T. Möller, M. Nagel, H. Borchert, S. G. Hickey, H. Weller, *J. Phys. Chem. B*, 2005, **109**, 17422-17428.
23 F. Auer, G. Nelles, B. Sellergren, *Chem. Eur. J.* 2004, **10**, 3232-3240.
24 H. Virieux, M. Le Troedec, A. Cros-Gagneux, W.-S. Ojo, F. Delpech, C. Nayral, H. Martinez, B. Chaudret, *J. Am. Chem. Soc.*, 2012, **134**, 19701-19708.
25 M. Barber, J. A. Connor, M. F. Guest, I. H. Hiller, M. Schwarz, M. Stacey, *J. Chem. Soc., Faraday Trans. 2,* 1973, **69**, 551-558.
26 Y. Li, G. Chen. Q. Wang, X. Wang, A. Zhou, Z. Shen, *Adv. Funct. Mater.*, 2010, **20**, 3390-3398.
27 G. Konstantatos, L. Levina, A. Fischer, E. H. Sargent, *Nano Lett.*, 2008, **8**, 1446-1450.
28 P. E. Laibinis, G. M. Whitesides, D. L. Allara, Y.-T. Tao, A. N. Parikh, R. G. Nuzzo, *J. Am. Chem. Soc.*, 1991, **113**, 7152-7167.
29 L. G. Mar, P. Y. Timbrell, R. N. Lamb, *Thin Solid Films*, 1993, **223**, 341-347.
30 J. Park, S.-W. Kim, *J. Mater. Chem.*, 2011, **21**, 3745-3750.
31 L. De Trizio, M. Prato, A. Genovese, A. Casu, M. Povia, R. Simonutti, M. J. P. Alcocer, C. D'Andrea, F. Tassone, L. Manna, *Chem. Mater.*, 2012, **24**, 2400-2406.
32 Z. Li, H. Dong, Y. Zhang, T. Dong, X. Wang, J. Li, X. Fu, *J. Phys. Chem. C*, 2008, **112**, 16046-16051.